A Fast and Direct Analysis of Three-Phase Induction Motors Using Finite Element

Matteo Carbonieri, Nicola Bianchi and Luigi Alberti

***Abstract*—A new finite-element technique for squirrel cage Induction Motor features analysis is presented in this paper. Motor performances are directly predicted performing on-load test simulations, in several working points. The finite-element analyses are carried out imposing both stator and rotor currents. Thus, only magnetostatic simulations are needed to get the electromagnetic quantities, such as torque and slip. Saturation phenomena can be considered in any operating conditions under load, with short computational time. In each motor working point, a very fast finite-element procedure, closely linked with the analytical machine model, is used to catch the proper current distribution in stator and rotor slots. It allows the motor performances to be predicted without the preliminary knowledge of the machine equivalent circuit parameters. Experimental tests are carried out and reported in order to verify analysis results.**

***Index Terms*—AC machine, Induction Motor, Finite Element Analysis, Modelling, Equivalent Circuit, Computational Efficient IM Analysis.**

I. Introduction

The Induction Motor (IM) is largely used in many applications, thanks to its low cost, good torque density and robustness. Despite the motor structure semplicity, the study of electromagnetic phenomena, that occur inside the machine, is complex [1]–[3]. For instance, on the IM rotor, a squirrel cage winding is often placed, whose behaviour is not the same as a common three-phase distributed winding, considering the current distribution. Further, the induced currents in the cage bars depend upon the relative speed between rotor and stator main field. The frequency of rotor electric quantities is not zero, then the rotor field position with respect to the magnetizing air-gap flux density, is affected by the rotor bar impedance angle.

The IM is easily analyzed using its equivalent circuital model, where the rotor cage impedance is referred to one phase of the stator. This analytical approach is well known and commonly used for a first estimation of motor performances [4]–[7]. The Finite Element Analysis (FEA) can improve the IM equivalent circuit derivation. It allows the complex saturation phenomena, that occur in no-load operations, to be better considered [8]–[11]. The IM equivalent circuit 3-D parameters, as the stator end-winding leakage inductance and the rotor rings resistance, can be computed using analytical models [12]–[14].

M. Carbonieri, N. Bianchi and L.Alberti are with the Department of Electrical Engineering, University of Padova, Padova, Italy (e-mail: edlab@dii.unipd.it)

When the IM works under load, the interaction between stator and rotor fields produces the motor torque and determines the net flux density in the air-gap. The machine exhibits a saturation map different from the no-load one, owing to high local saturations, scattered especially in the tooth tips. Direct test simulations allows the on-load saturation to be well considered in the computation of the equivalent circuit lumped parameters and motor performances [14], [15].

The aim of the paper is to predict the steady-state performance of a squirrel cage IM, performing FEA, where both stator and rotor currents are imposed as field sources. The key point of the procedure is to make FE analyses closely connected with the motor analytical model with the purpose of getting the proper stator and rotor current distribution in the motor working under-load.

This technique allows the electromagnetic torque and slip to be achieved by means of only magnetostatic FE simulations. The advantage is twofold: iron saturation is well considered in any working point and computational time is short, avoiding complex time-stepping analyses.

Hereafter the on-load direct analysis approach is used for a double cage motor characterization. However, this technique can be applied to analyze IMs with any type of rotor, such as closed slot squirrel cage and wound rotor machines.

In presence of cage rotor motor, three-phase equivalent winding, with the same behavior as the squirrel cage, is a useful tool for imposing the proper rotor electric load and computing the rotor flux linkages. In order to prove the accuracy of the proposed analysis strategy, a comparison with measurements is reported at the end of the paper.

II. Rotor Equivalent Three-Phase Winding.

In the instant time t, ω_{sl}^{e} is the relative mechanical speed between the stator field and the rotor, in electric radiants per second. Considering a sinusoidal air-gap flux density distribution, the induced voltage, at the terminals of each rotor bar, can be expressed as:

$$\begin{cases} e_1(t) = \widehat{B}_{\mathrm{g}} \sin\left(\omega_{sl}^{e}\, t\right) L_{\mathrm{stk}} \dfrac{D_{\mathrm{i}}}{2} \omega_{sl}^{e} \\ \vdots \\ e_{Q_r}(t) = \widehat{B}_{\mathrm{g}} \sin\left(\omega_{sl}^{e}\, t - (Q_r - 1)\alpha_{sr}^{e}\right) L_{\mathrm{stk}} \dfrac{D_{\mathrm{i}}}{2} \omega_{sl}^{e} \end{cases} \tag{1}$$

where α_{sr}^{e} is the electrical rotor slot angle, Q_r is the rotor slot number, D_{i} and L_{stk} are the inner diameter and the stack

length. Rotor bar currents can be written as following:

$$\begin{cases} i_1(t) = \widehat{B}_{\mathrm{g}} \sin\left(\omega_{sl}^e\, t - \phi_r\right) \dfrac{D_{\mathrm{i}}\, L_{\mathrm{stk}}\, \omega_{sl}^e}{2|\dot{z}_{\mathrm{bar}}|} \\ \vdots \\ i_{Q_r}(t) = \widehat{B}_{\mathrm{g}} \sin\left(\omega_{sl}^e\, t - (Q_r-1)\alpha_{sr}^e - \phi_r\right) \dfrac{D_{\mathrm{i}}\, L_{\mathrm{stk}}\, \omega_{sl}^e}{2|\dot{z}_{\mathrm{bar}}|} \end{cases} \tag{2}$$

where $\dot{z}_{\mathrm{bar}} = |\dot{z}_{\mathrm{bar}}| e^{j\phi_r}$ is the equivalent bar impedance $\dot{z}_{\mathrm{bar}}$, that takes into account the presence of cage short-circuit rings.

Fig. 1 shows that, when only the main harmonic of airgap flux is considered, spatial behavior of induced voltage and current, in the rotor bars, exhibits almost a sinusoidal waveform.

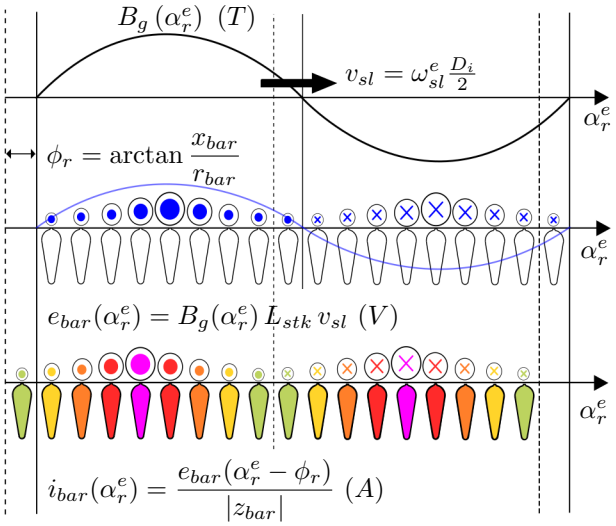

Fig. 1. Induced voltage and current spatial distribution in the slots of a squirrel cage rotor. In the drawing, v_{sl} indicates the relative speed between the air-gap flux density and the rotor, in meters per second; α_r^e is the rotor electrical angle.

An interesting trick is considering a three-phase rotor equivalent winding sinusoidally distributed in the rotor slots. Fig. 2 shows a sketch of such a three-phase rotor winding. The shading indicates the theoretical conductor density belonging to each phase within the rotor slots. Forcing a three-

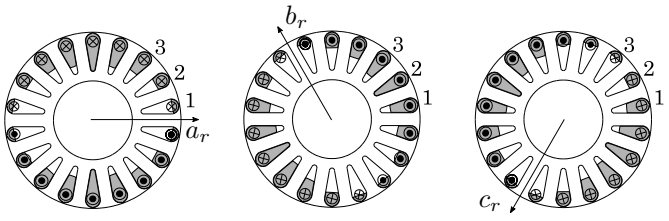

Fig. 2. Sketch of the three-phase equivalent rotor winding.

phase current in the equivalent rotor winding, the sinusoidal current distribution in the rotor slots, is reproduced. The vectors k_{ra}, k_{rb} and k_{rc} define the fill factor of any rotor slot, according to a given phase:

$$\begin{aligned} k_{ra,i} &= \sin\left(\alpha_{sr}^e/2 + \alpha_{sr}^e(i-1)\right); \\ k_{rb,i} &= \sin\left(\alpha_{sr}^e/2 + \alpha_{sr}^e(i-1) - 2\pi/3\right) \\ k_{rc,i} &= \sin\left(\alpha_{sr}^e/2 + \alpha_{sr}^e(i-1) - 4\pi/3\right) \end{aligned} \tag{3}$$

where $i = 1, \ldots, Q_r$. The rotor winding factor is computed as following:

$$k_{wr} = \frac{\sqrt{\left(\sum_{i=1}^{Q_r} k_{ra,i} \cos\left(\frac{2i-1}{2}\alpha_{sr}^e\right)\right)^2 + \left(\sum_{i=1}^{Q_r} k_{ra,i} \sin\left(\frac{2i-1}{2}\alpha_{sr}^e\right)\right)^2}}{\sum_{i=1}^{Q_r} k_{ra,i}} \tag{4}$$

Theoretically, the winding factor of a sinusoidally distributed winding is equal to $\pi/4$.

The number of conductors per phase of the rotor winding is fixed in order to have the same number of effective conductors as the stator winding:

$$N_r\, k_{wr} = N_s\, k_{ws} \tag{5}$$

where N_s is the number of conductors per phase of the stator winding and k_{ws} is the stator winding factor. The equivalence (5) accounts to facilitate the parameter estimation of the equivalent circuit. The number of series conductors per phase in each rotor slot results in:

$$\begin{aligned} n_{csr,a} &= \frac{N_r}{\sum_{i=1}^{Q_r} k_{ra,i}} k_{ra}; \quad n_{csr,b} = \frac{N_r}{\sum_{i=1}^{Q_r} k_{rb,i}} k_{rb} \\ n_{csr,c} &= \frac{N_r}{\sum_{i=1}^{Q_r} k_{rc,i}} k_{rc} \end{aligned} \tag{6}$$

The condition (4) makes the stator and rotor synchronous inductance to be almost the same. They differ from the leakage component, whilst the magnetizing component is the same:

$$\begin{aligned} L_{Ms} &= \frac{3}{\pi}\mu_0 \left(\frac{N_s\, k_{ws}}{2p}\right)^2 \frac{D_{\mathrm{i}}\, L_{\mathrm{stk}}}{g''} \\ L_{Mr} &= \frac{3}{\pi}\mu_0 \left(\frac{N_r\, k_{wr}}{2p}\right)^2 \frac{D_{\mathrm{i}}\, L_{\mathrm{stk}}}{g''} \end{aligned} \tag{7}$$

where g'' is the magnetic airgap, that takes into account the iron saturation and the Carter coefficient. It follows:

$$L_M = L_{Ms} = L_{Mr}$$

III. IM EQUIVALENT MODEL.

The challenge of simulating the IM under load, using magnetostatic analyses, is to understand the proper relative position of stator and rotor electric loads in any working condition. For this reason the analytical model has to be strictly connected with FEA. The IM steady-state vector equations are [6], [7]:

$$\begin{aligned} \vec{v}_s &= R_s \vec{i}_s + \mathrm{j}\omega_s \left(L_s \vec{i}_s + M \vec{i}_r\right) \\ 0 &= \frac{R_r}{s} \vec{i}_r + \mathrm{j}\omega_s \left(L_r \vec{i} + M \vec{i}_s\right) \end{aligned} \tag{8}$$

where L_s and L_r are the stator and rotor self inductance and M is the mutual synchronous inductance. The equations in (8) are linked with the mutual coupling equivalent circuit in Fig. 3(a). The transformation constant $\mathbf{t}$ can be chosen equal to the ratio between the stator and rotor effective number of conductors. Considering (5) it results $\mathbf{t} = n = 1$ and the T-form of the equivalent circuit (Fig. 3(b) top) is derived, where L_{ls} and L_{lr} are the stator and rotor leakage inductances.

Further the mutual synchronous inductance results the same as the magnetizing component of stator and rotor self inductances [7]:

$$M = L_M \tag{9}$$

Considering (9), imposing $\mathbf{t}$ equal to:

$$n' = M/L_r = L_M/L_r \tag{10}$$

the inverse-Γ circuit can be obtained (Fig. 3(b) bottom). The related steady-state space vector diagram is shown in Fig. 4. The rotor flux linkage space vector $\vec{\lambda}_r$ lies along the $d-$axis.

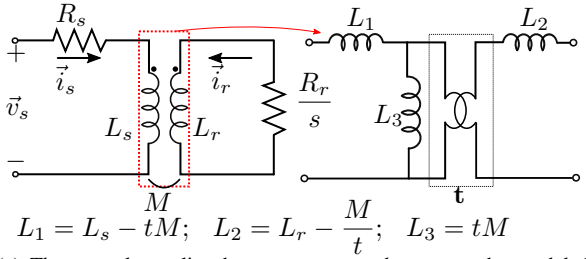

(a) The mutual coupling between stator and rotor can be modeled using a grid of inductances with the ideal transformer.

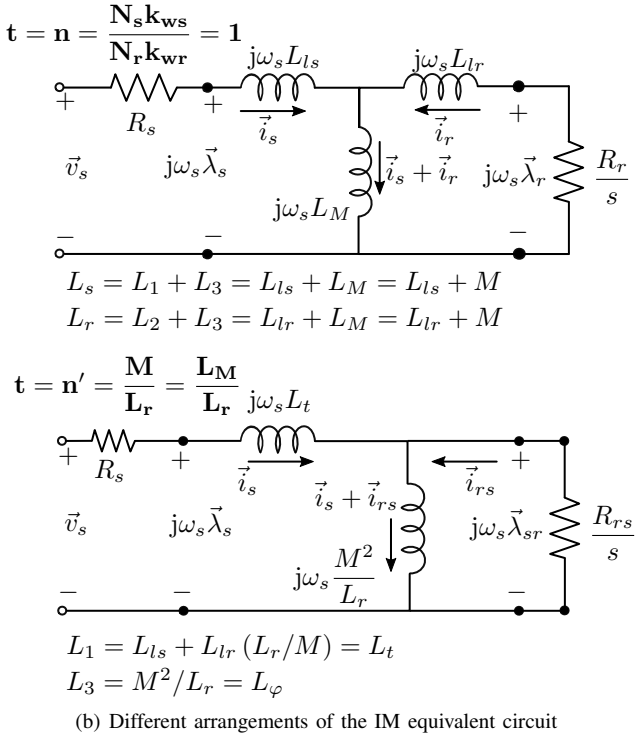

(b) Different arrangements of the IM equivalent circuit

Fig. 3. The choice of the transformation ratio t leads to different configurations of the equivalent circuit. In the T-form, with $n = 1$, the rotor current is already referred to the stator. The same for $\vec{\lambda}_r$ and the rotor parameters.

Stator and rotor current vectors, considering the inverse-Γ model, are:

$$\vec{i}_s = i_{sd} + \mathrm{j}i_{sq} = i_\mu + \mathrm{j}i_\tau; \quad \vec{i}_r = \mathrm{j}i_{rq} = -\mathrm{j}i_\tau \frac{M}{L_r} \tag{11}$$

The real part of the stator current, i_μ, is the magnetizing current, that produces stator and rotor main flux linkages. The imaginary part of stator current, i_τ, is the torque current, that occurs when the motor is loaded.

Analyzing the motor according to the inverse-Γ model, stator and rotor flux linkages, in the synchronous reference frame, are given by:

$$\begin{aligned} &\lambda_{sd} = L_s i_\mu; \quad \lambda_{sq} = \left(L_{ls} + L_{lr}\frac{M}{L_r}\right) i_\tau \\ &\lambda_{rd} = M i_\mu; \quad \lambda_{rq} = 0 \end{aligned} \tag{12}$$

The main advantage of the inverse-Γ model is that the stator and rotor main flux linkages λ_{sd} and λ_{rd} are due only to the real part of the stator current i_μ, for this reason the inverse-Γ model is particularly suitable to be linked with

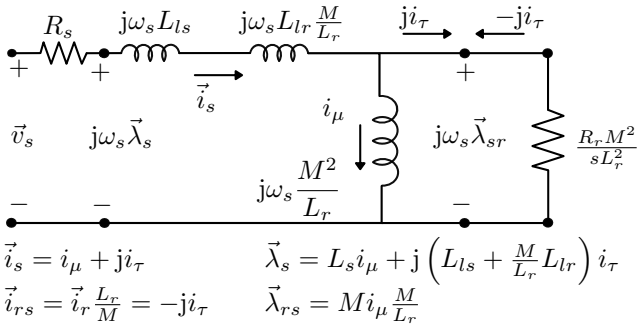

(a) Inverse Γ form of the IM equivalent circuit, using space vectors.

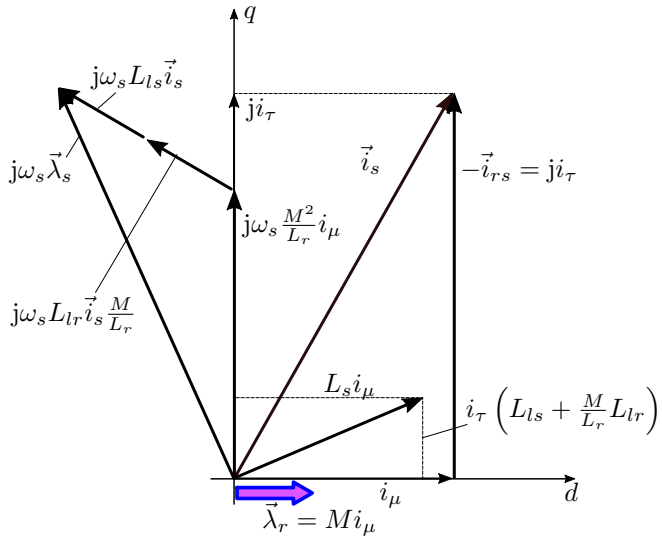

(b) Vector diagram of the machine in the synchronous reference frame related to the inverse-Γ model. At steady-state, all space vectors rotate, with respect to the stationary reference frame, at the angular frequency ω_s

Fig. 4. The inverse-Γ equivalent circuit at steady-state is linked with the space vector diagram in the synchronous reference dq, in which the rotor flux space vector lies along the d-axis.

FEA. Once the flux λ_{rd} has been created, the motor torque is determined by the imaginary component:

$$T = \frac{3}{2}\, p\, \frac{M^2}{L_r}\, i_\mu\, i_\tau \tag{13}$$

From the rotor voltage equation (8) the slip can be achieved as:

$$s = \frac{(3/2)\, R_r\, (i_\tau \cdot n')^2}{(3/2)\, \omega_s \lambda_{rd}\, (i_\tau \cdot n')} = \frac{P_{Jr}}{P_{trans}} \tag{14}$$

where P_{Jr} are the Joule losses in the rotor cage and P_{trans} is the transmitted power to the rotor.

IV. FEA Procedure

The on-load analysis is carried out considering the time instant in which the rotating dq reference frame overlaps the $\alpha\beta$ plane, as shown in Fig. 5. Stator and rotor current vectors are set in the $\alpha\beta$ reference frame for magnetostatic FEA.

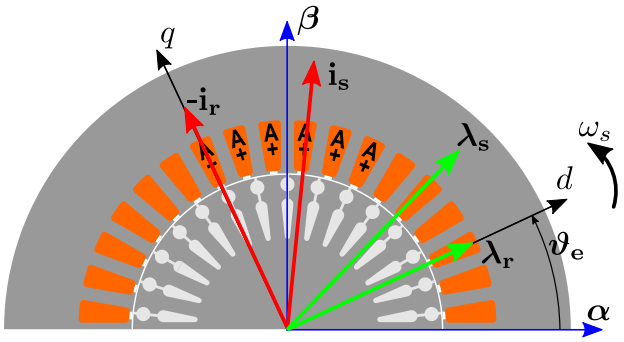

Fig. 5. The machine stationary reference frame $\alpha\beta$ oriented with stator a magnetic axis. The time instant in which dq overlaps $\alpha\beta$ is considered. Stator and rotor current vectors can be forced in $\alpha\beta$. Current values are set in order to verify the analytical hypothesis $\lambda_{r\beta} = 0$.

The inverse-Γ model condition $\lambda_{r\beta} = 0$ has to be verified using FE, in each analyzed working point, in order to proper connect FEA with the inverse-Γ model. The following relationship between stator and rotor $\beta-$axis currents has to be imposed:

$$i_{r\beta} = -\frac{M}{L_r} i_{s\beta} \tag{15}$$

A two steps FE procedure is necessary to get the proper rotor current and the motor performances. In the first simulation, inductances M and $L_r = M + L_{lr}$ are computed taking into account carefully the iron saturation. In the second FEA the condition (15) is imposed, the electromagnetic torque and rotor Joule losses are directly computed from the field solution. The slip is derived using (14), for a certain value of the electric angular frequency ω_s. In Fig. 6, the procedure scheme is shown.

All the on-load magnetostatic simulations are carried out imposing both stator and rotor current. The non-uniform current distribution in rotor bars is neglected. This is a reasonable assumption for operation close to nominal speed, where the slip, and so the rotor frequency, is low.

At first, no-load simulations are performed in order to estimate the stator magnetizing current i_μ at rated voltage and frequency. Only α-axis stator current is imposed for no-load analysis. In Fig. 6, the no-load flux lines do not cross the α-axis, thus stator flux linkage exhibits only the α-component.

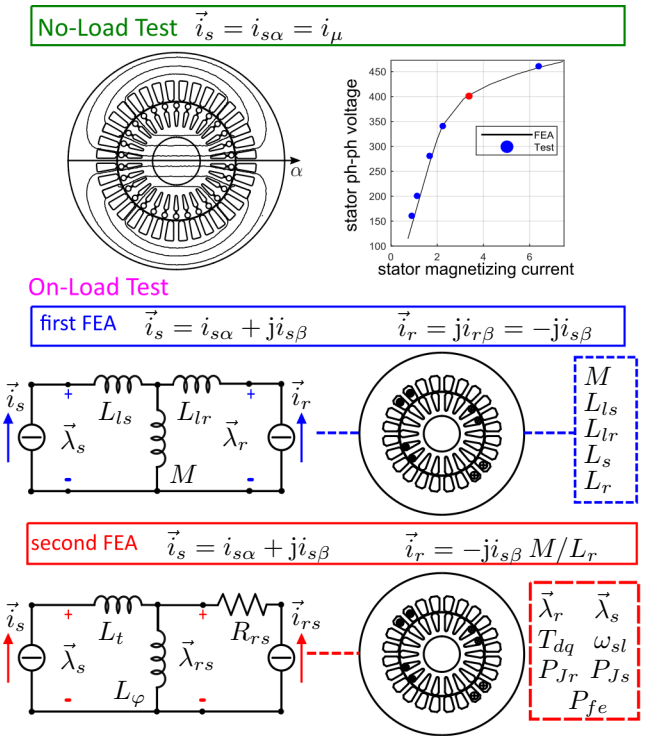

Fig. 6. FE procedure scheme. The no-load test is carried out to find the rated magnetizing current. In each on-load working point two steps analysis is necessary to get the motor performances.

In the simulations under load, besides the current i_μ, a β-axis current is imposed in stator winding. The related rotor current $i_{r\beta}$ has to be set using (15), in order to get the proper operating condition according to the analytical model.

Several on-load working points are investigated, increasing the stator torque current $i_{s\beta} = i_\tau$.

In the first step of the on-load analysis procedure, inductances M and L_r have to be computed. Stator and rotor current vectors, forced in the machine, in the first simulation, are:

$$\begin{aligned} \vec{i}_s &= i_{s\alpha} + \mathrm{j}i_{s\beta} = i_\mu + \mathrm{j}i_\tau; \\ \vec{i}_{r,1} &= \mathrm{j}i_{r\beta} = -\mathrm{j}i_\tau \end{aligned} \tag{16}$$

where the rotor α-axis current is set to zero. The T-form equivalent circuit parameters can be derived. In particular, the leakage inductances L_{ls} and L_{lr} can be separated from the magnetizing component M of L_s and L_r. Stator and rotor flux linkages, considering current vectors in (16) are analytically expressed as:

$$\begin{aligned} \vec{\lambda}_s &= L_s \vec{i}_s + M\vec{i}_r = L_s i_\mu + \mathrm{j}L_{ls} i_\tau; \\ \vec{\lambda}_r &= M\vec{i}_s + L_r \vec{i}_r = M i_\mu - \mathrm{j}L_{lr} i_\tau \end{aligned} \tag{17}$$

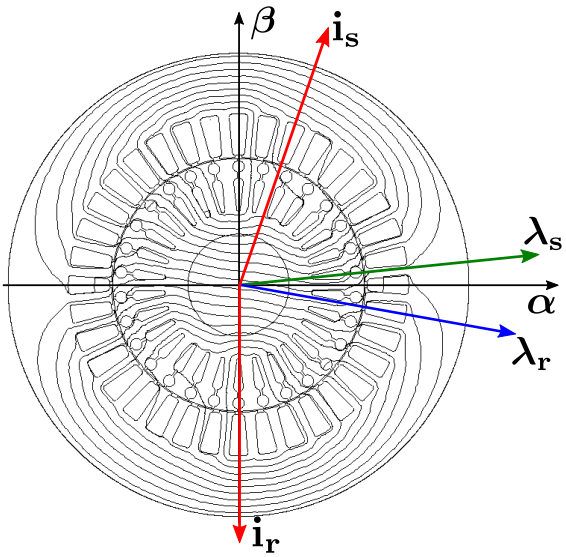

Fig. 7. First simulation field solution flux lines. Imposing $i_{s\beta} = -i_{r\beta}$, the rotor flux linkage along β-axis is not zero.

In Fig. 7, the first simulation field solution is reported. The flux lines widely cross the α-axis, the rotor flux $\lambda_{r\beta}$ is not equal to zero.

In Fig. 8, the flux lines, due to stator and rotor currents along α and β axes, are split and put in evidence.

In Fig. 8(a) it is shown that the machine magnetizing field is produced by the stator current along the α-axis. In Fig. 8(b) resulting leakage flux lines are shown, when stator and rotor β-axis currents are equal and opposite.

Stator and rotor flux linkage space vectors are derived from the first FEA field solution. The inductances in the T-form of equivalent circuit can be achieved as:

$$L_{ls} = \frac{\lambda_{s\beta}}{i_\tau}; \quad L_{lr} = \frac{\lambda_{r\beta}}{-i_\tau}; \quad M = \frac{\lambda_{r\alpha}}{i_\mu} \tag{18}$$

The relationship (15), between stator and rotor β-axis currents, has to be applied, using the inductances computed in (18), in order to set $\vec{\lambda}_r$ along the α axis, according to the inverse-Γ model.

The rotor synchronous inductance is derived as: $L_r = M + L_{lr}$. The stator current does not change, whilst the rotor β-axis current is corrected to perform a second FEA. The stator and rotor current vectors in the second simulation are:

$$\begin{aligned} \vec{i}_s &= i_{s\alpha} + \mathrm{j} i_{s\beta} = i_\mu + \mathrm{j} i_\tau \\ \vec{i}_{r,2} &= \mathrm{j} i_{r\beta} = -\mathrm{j} i_\tau \frac{M}{L_r} \end{aligned} \tag{19}$$

In Fig. 10, the second simulation field solution is shown. It is worth to notice that the flux lines within the rotor are almost parallel to the α-axis, which means that $\lambda_{r\beta} \approx 0$.

Stator and rotor currents are imposed according to the inverse-Γ equivalent model, the torque and the rotor Joule losses are achieved from the second FEA field solution. The slip can be computed using (14), where $\lambda_{rd} = \lambda_{r\alpha}$ is derived

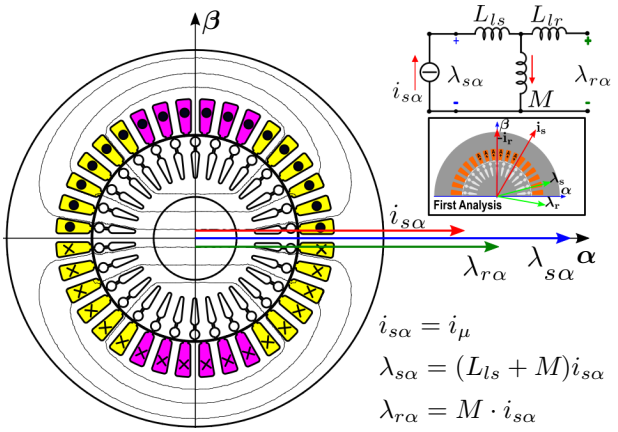

(a) First simulation, α-axis flux lines. Only the stator current i_μ acts along the α-axis. It yields the magnetizing component of stator and rotor flux linkages: Mi_μ. The magnetizing field flux lines are shown.

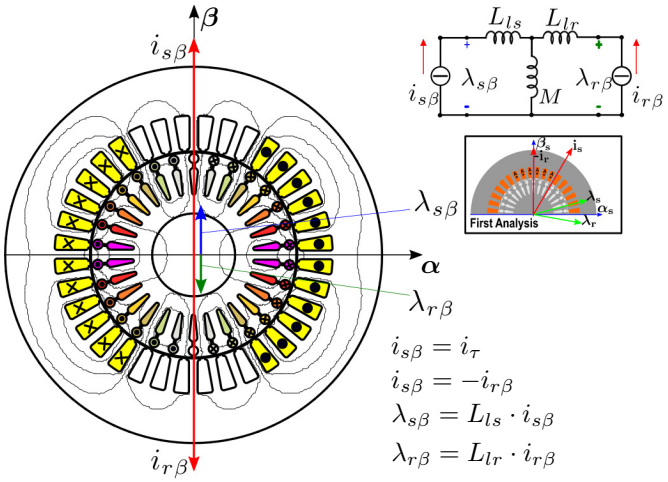

(b) First simulation, β-axis flux lines. Along β axis stator and rotor currents are equal and opposite. Leakage fluxes determine the β component of stator and rotor flux linkages.

Fig. 8. Currents and fields acting along two axis in the first FEA simulation.

by means of the magnetic vector potential and ω_s is the rated electric angular frequency.

Let's compare Fig. 9(a) and Fig. 9(b). In the first, leakage flux lines are linked with stator and rotor winding, according to leakage inductances L_{ls} and L_{lr}, when $i_{s\beta} = -i_{r\beta}$. In the second, stator β current has been corrected, using (15). In this case, the most of the β leakage flux lines are linked with the stator winding. Notice that, using the inverse-Γ equivalent model, the rotor leakage flux is referred to the stator and leakage flux $\lambda_{s\beta}$ is related to the global leakage inductance L_t:

$$\lambda_{s\beta} = L_t i_{s\beta} = \left(L_{ls} + L_{lr} \frac{M}{L_r} \right) i_{s\beta} \tag{20}$$

In order to improve the simulation accuracy, the effective iron length is considered: $L_{\mathrm{fe}} = k_{\mathrm{pack}} L_{\mathrm{stk}}$, where k_{pack} is the packing coefficient. The electromagnetic torque and flux linkages are derived considering the iron length L_{fe}. Instead, the rotor Joule losses computed from FE solution, P_{Jr}^{FE}, has

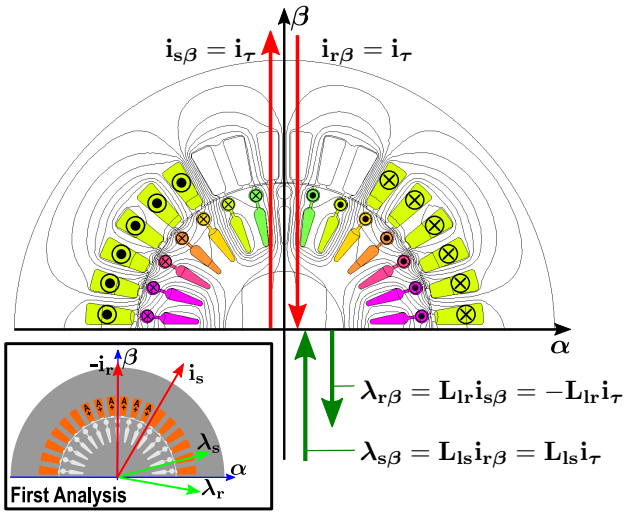

(a) Leakage fluxes in the field solution when the stator and rotor current vector are: $\vec{i}_s = \mathrm{j}i_{s\beta} = \mathrm{j}i_\tau$ and $\vec{i}_r = \mathrm{j}i_{r\beta} = -\mathrm{j}i\tau$. In this situation the rotor flux linkage $\lambda_{r\beta}$ is no zero.

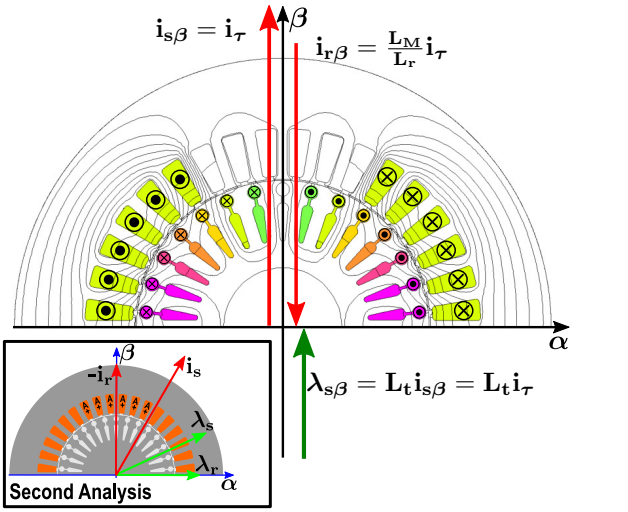

(b) Leakage fluxes in the field solution when the stator and rotor current vector are: $\vec{i}_s = \mathrm{j}i_{s\beta} = \mathrm{j}i_\tau$ and $\vec{i}_r = \mathrm{j}i_{r\beta} = -\mathrm{j}i\tau\,(M/L_\tau)$. The most of the leakage flux lines are linked with the stator winding. The roto flux $\lambda_{r\beta} \simeq 0$.

Fig. 9. Flux lines due to β-axis stator and rotor currents imposed, in (a), equal and opposite. In (b) $i_{r\beta} = n'\, i_{s\beta}$

to be corrected as $P_{Jr} = P_{Jr}^{\mathrm{FE}}/k_{\mathrm{pack}}$, to take into account that the rotor bars resistance depends upon the pack length L_{stk}.

V. Application and Measurements Comparison

The presented procedure has been used to analyze a 2-pole, 11 kW, double-cage IM. The performances are predicted in several working points at the rated voltage and frequency of 400 V, 50 Hz. The stator winding is full pitched with six slots per pole per phase. Measurements have been done increasing the torque from 25% up to 150% of the rated value of 35 N m.

In Fig. 10 the on-load field solution in the rated working point is shown.

Once the on-load field problem is solved, the voltage is

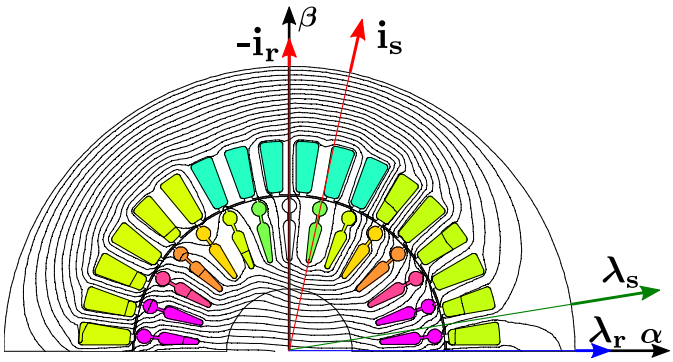

Fig. 10. On-load simulations result in the rated working point. A sketch of the vector diagram is reported as well. Flux lines in the rotor are almost parallel to the α-axis, since the flux $\lambda_{r\beta} \simeq 0$. The stator flux space vector is shifted, due to the imaginary component along β-axis.

TABLE I
FEA results increasing rotor torque current.

T_{FE} (N m)	V_{FE} (V)	i_μ (A)	$i_{r\beta}$ (A)	$i_{s\beta}$ (A)	$\lambda_{r\beta}$ (μWb)
8.3	399	3.11	2.29	2.3	0.098
16.6	399	3.08	4.57	4.61	0.88
24.8	400	3.04	6.86	6.91	3.0
32.9	400	2.99	9.12	9.19	2.9
40.8	399	2.95	11.45	11.55	5.6
48.6	398	2.92	13.72	13.88	26

computed from stator flux linkages, imposing the actual value of the angular frequency. The effect of the stator end-winding leakage inductance and resistance are considered in the voltage computation. Increasing torque current, the voltage drop on the stator impedance increases. The stator magnetizing current has been decremented in each working point, to take into account the on-load voltage drop, in order to keep constant the stator winding voltage, equal to the rated one. In Table I FEA results are reported in several working points. The resulting voltage from FEA is equal to the rated on in each on-load operation. The values of β-axis rotor flux in the analyzed working points, are reported together with stator and rotor current components along α and β.

TABLE II
Motor performances measured in several on-load working point with FEA results comparison.

Load	slip (%)	T_{meas} (N m)	T_{FE} (N m)	$I_{\mathrm{s,meas}}$ (A)	$I_{\mathrm{s,FE}}$ (A)
25%	0.75	10	9.4	4.3	4.1
50%	1.48	18.5	18.3	6.2	5.9
75%	2.29	28	27.9	8.7	8.3
100%	3.10	37	37.2	11.3	10.8
125%	3.90	44.6	45.8	13.6	13.3
150%	4.60	51	52.8	15.6	15.4

In Fig. 11 and Table II data from measurements are compared with FEA results. The good agreement between direct

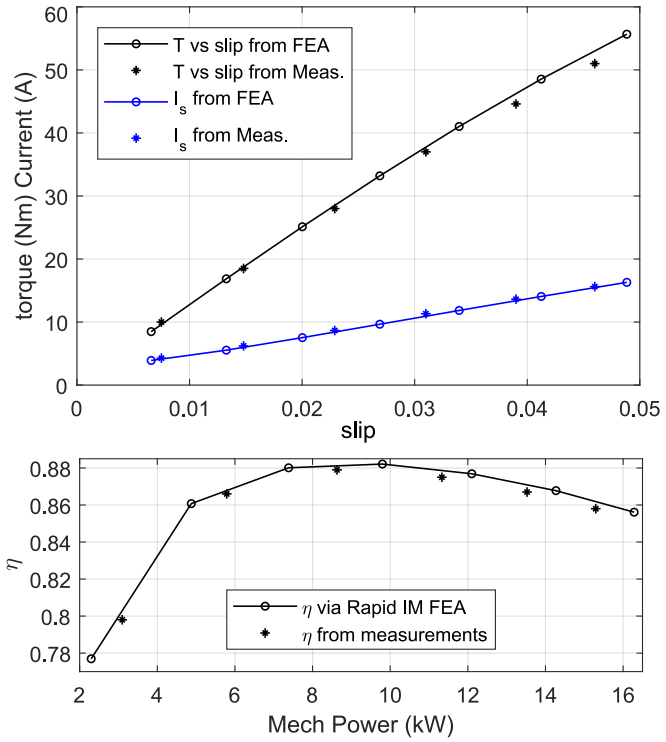

Fig. 11. FEA results and measurements comparison. The torque versus speed characteristic and the efficiency have been computed according to the current standard

test simulations and measurements, proves the accuracy of the analysis strategy, in all the operating conditions investigated.

VI. Conclusions

A new analysis procedure to quickly predict the IM performances, has been presented. The analytical machine model is closely linked with FEA, in order to properly set stator and rotor currents in on-load simulation. The iron saturation is well considered in any working points, both in no-load and under load condition.

The analyzed motor is supplied by a constant voltage source, thus no-load FE analyses are required to estimate the magnetizing current at rated voltage and frequency. In this paper, the analysis strategy has been applied for an IM fed by the grid. The method can be useful to predict the steady-state performances of a controlled IM. The analysis technique is based only upon magnetostatic simulations, that makes the computation time short. Further, the connection with analytical model makes the process to get the right value of stator and rotor currents fast and easy: only two simulations are required to get the proper operating condition, according to the analytical model.

The lumped parameters of the equivalent circuit in Fig. 4(a) can be computed from FE solutions. Both the inverse-Γ and the T form of the IM circuit can be built. In particular, the definition of a rotor equivalent three-phase winding allows the mutual inductance between stator and rotor and the rotor leakage inductance to be easily computed performing magnetostatic FEA.

The agreement between measurements and FEA results proves the accuracy of the proposed strategy.

References

[1] C. Veinott, *Theory and Design of Small Induction Motors*. New York: McGraw-Hill, 1959.

[2] I. Boldea, S. A. Nasar, *The Induction Machine Handbook*, ser. Power Electronics and Applications Series. Boca Raton, FL: CRC Press, 2001.

[3] M. Liwshitz-Garik and C. C. Whipple, *Electric Machinery, Vol. II, A-C Machines*, New York: Van Nostrand, 1960.

[4] P. Alger, *Induction Machines, Their Behaviour and Uses*. 2nd ed. Paris, France: Gordon and Breach, 1970.

[5] T. Lipo *Introduction to AC Machine Design*. Wisconsin Power Electronics Research Center, Univ. of Wisconsin, 2007.

[6] D. Novotny, T. Lipo *Vector Control and Dynamics of AC Drives*. New York: Oxford Univ. Press, 1996.

[7] G. R. Slemon, "Modelling of induction machines for electric drives," *IEEE Transactions on Industry Applications*, vol. 25, no. 6, pp. 1126–1131, Nov./Dec. 1989.

[8] S. Williamson and J. Ralph, "Finite–element analysis of an induction motor fed from a constant–voltage source," *IEE Proc., Pt. B*, vol. 130, no. 1, pp. 18–24, Jan. 1983.

[9] S. Williamson, A. Smith, M. Begg, and J. Smith, "General techniques for the analysis of induction machines using finite elements," in *Proc. of International Conference on Evolution and Modern Aspect of Induction Motors*, Turin, Italy, July 8–11 1986, pp. 389–395.

[10] S. Williamson, M.J. Robinson, "Calculation of Cage Induction Motor Equivalent Circuit Parameters using finite elements," in *IEE PROCEEDINGS–B, Vol. 138, No. 5, September 1991.*

[11] A. Arkkio, "Analysis of induction motors based on the numerical solution of the magnetic field and circuit equations," Ph.D. Thesis, Helsinki University of Technology, Helsinki, Finland, Laboratory of Electromechanics, 1987, acta Polytechnica Scandinava, Electr. Eng. Series No.59.

[12] L. Alberti, N. Bianchi, S. Bolognani, "A very rapid prediction of IM performance combining analytical and finite-element method," *IEEE Transactions on Industry Applications*, vol. 44, no. 5, pp. 1505–1512, Sep./Oct. 2008.

[13] N. Bianchi, S. Bolognani, G. Comelato "Finite element analysis of three-phase induction motor: Comparison of two different approaches," *IEEE Transactions on Industry Applications*, vol. 14, no. 4, pp. 1523–1528, Dec. 1999.

[14] L. Alberti, N. Bianchi, S. Bolognani "Variable-Speed Induction Machine Performance Computed Using Finite-Element," *IEEE Transactions on Industry Applications*, vol. 47, no. 2, Mar/Apr. 2011.

[15] A. Stermecki, O. Biro, K. Preis, S. Rainer, K. Krischan, G. Ofner, "Computation of load-dependent equivalent circuit parameters of squirrel cage induction motor using time-harmonic FEM," in *Proc. 18th ICEM,* Vilamaura, Portugal, Sep. 2008, pp. 1-6.

VII. Biographies

Matteo Carbonieri received the Master degree in electrical engineering from the University of Padova, Padova, Italy, in 2017. He is currently Ph.D. student in the Electric Drives Laboratory, University of Padova, working on the design and analysis of electric machines.

Nicola Bianchi was born in Verona, Italy, in 1967. He received the Laurea and Ph.D. degrees in electrical engineering from the Department of Electrical Engineering, University of Padova, Padova, Italy, in 1991 and 1995, respectively. Since 1998, he has been an Assistant Professor in the Electric Drives Laboratory, Department of Electrical Engineering, University of Padova. His research activity is in the field of the design of electrical motors for electric drive applications.

Luigi Alberti received the Laurea and Ph.D. degrees in electrical engineering from the University of Padova, Padova, Italy, in 2005 and 2009, respectively. He is currently an Assistant Professor in the Electric Drives Laboratory, University of Padova, working on the design, analysis, and control of electric machines. He is also a consultant to various industries.